

Interaction between a crack and a circular inhomogeneity with interface stiffness and tension

Sofia G. Mogilevskaya · Steven L. Crouch · Roberto Ballarini · Henryk K. Stolarski

Received: 18 March 2009 / Accepted: 4 August 2009 / Published online: 3 September 2009
© Springer Science+Business Media B.V. 2009

Abstract The interaction between a straight crack and a circular inhomogeneity with interface stiffness and energy is considered. The Gurtin and Murdoch model is adopted, wherein the interface between the inhomogeneity and the matrix is regarded as a material surface that possesses its own mechanical properties and surface tension. The elastostatics problem is decomposed into two complimentary problems for (1) a circular disk with unknown distributions of traction and displacements along its boundary and (2) a loaded isotropic plane containing a circular hole with unknown distributions of traction and displacements along its boundary. The unknown distributions are determined through the application of the constitutive relations at the material surface. For selected values of the dimensionless parameters that quantify the geometry, material properties and applied loading, the stress field, stress intensity factors and energy release rates are calculated using a complex boundary integral equation approach. Particular attention is paid to crack-tip shielding and anti-shielding that develops as a result of the stresses introduced by the material surface. An illustrative example involving a perforated plate loaded in tension suggests that the material surface produces a modest level of expected effective toughening.

Keywords Circular inhomogeneity · Gurtin and Murdoch model · Surface tension · Surface elasticity · Straight crack · Complex boundary integral equation

1 Introduction

This paper presents the results of a two-dimensional elastostatics analysis of the effects of surface stress on the interaction between a matrix crack and a circular inhomogeneity. The surface stress is accounted for through the Gurtin and Murdoch model of a material surface (Gurtin and Murdoch 1975, 1978), wherein the interface between the matrix and the inhomogeneity is regarded as a material surface possessing its own elasticity and surface tension. Particular attention is paid to the potential reduction in flaw sensitivity of the matrix resulting from the residual stresses produced just outside the inhomogeneity by the interface tension and elasticity.

The Gurtin and Murdoch model has received renewed attention because of the potential influence of surface effects on the mechanical properties and response of nanoscale structures that involve relatively large surface-to-volume ratios. Most applications of the model to date involve analyses of the stress fields produced by isolated spherical or cylindrical inhomogeneities embedded in an infinite or semi-infinite matrix (Miller and Shenoy 2000; Sharma and Ganti 2002, 2004; Sharma et al. 2003; Yang 2004; Duan et al. 2005a,b,c, 2006, 2007; He and Li 2006; Huang and Wang 2006;

S. G. Mogilevskaya (✉) · S. L. Crouch · R. Ballarini · H. K. Stolarski
Department of Civil Engineering, University of Minnesota,
500 Pillsbury Drive S.E., Minneapolis, MN 55455, USA
e-mail: mogil003@umn.edu

Lim et al. 2006; Mi and Kouris 2006; Chen et al. 2007; Zhang and Wang 2007; Tian and Rajapakse 2007a,b). Most of the papers, including Tian and Rajapakse (2007c) two-dimensional finite element method formulation for the analysis of multiple interacting anisotropic inhomogeneities, invoke simplifications of Gurtin and Murdoch's constitutive equations made by neglecting a whole or a part of the term associated with the gradient of surface displacement. Mogilevskaya et al. (2008) provided a basis for critical review of the significance to inhomogeneity problems of such simplifications by deriving the precise component forms of Gurtin and Murdoch's three-dimensional equations for interfaces of arbitrary shape, and applying the complete model to the two-dimensional problem of multiple, arbitrarily located, interacting circular inhomogeneities. They showed that the stress and strain fields in the vicinity of the interface are sensitive to the choice of the interface constitutive law.

Application of simplified forms of the Gurtin and Murdoch model to problems involving point defects and cracks include the analysis of interaction of an edge dislocation with a single inhomogeneity (Fang and Liu 2006; Fang et al. 2007), and the configurational equilibrium of isolated cracks and voids (Rajapakse 1975; Thomson et al. 1986; Chuang 1987; Wu 1999; Wu and Wang 2001). No results are available, however, for the interaction of a crack and an inhomogeneity. This open problem is worth exploring because the surface tension and surface elasticity produce residual stress fields in the vicinity of the material surface that can either suppress or enhance crack initiation and propagation within the matrix. He and Li's closed-form solution for the stress field produced by a spherical void in an infinite matrix demonstrated that significant tensile and compressive stresses develop just outside the void. Because the Gurtin and Murdoch model introduces an intrinsic length scale, the magnitude of the residual stresses increase with decreasing hole-size. For the representative parameters considered in their paper, the residual stress can approach the better part of a GPa.

This paper explores the expected amount of shielding/antishielding induced by the residual stress field on the tips of a matrix crack. The configuration considered involves a straight crack interacting with a circular inhomogeneity (Fig. 1). The surface effects are included only on the interface between the circular inhomogeneity and the matrix. Even though it is clear that those effects are also present on the surface of the

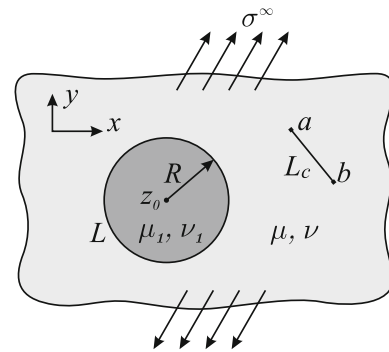


Fig. 1 Problem formulation

crack, their precise analysis is still elusive in spite of several past contributions in that area. Various possible modeling approaches have been discussed, for example, by Oh et al. (2006) but no systematic and widely accepted methodology of solving the problem has emerged. There are approximate methods of solving the problem of a crack with surface effects, such a very skillful approach presented by Wu (1999). However, his approach is based either on the overall energy considerations or includes surface effects approximately, by considering geometry of the deformed crack surfaces without those effects (acknowledging the difficulties with the systematic solution of the problem). Furthermore, his approach provides only the modifications to the stress intensity factors, which is not sufficient in the analysis of the complete boundary value problem, as done in this work. Thus, we have decided to consider a crack without surface effects in the believe that those effects (whatever they are) will be superposed with the effects that we discuss herein.

The formulation involves the superposition of two problems; (1) a circular disk with arbitrary traction and displacement conditions along its boundary (Fig. 2a), and (2) a loaded infinite matrix containing a crack interacting with a circular hole with arbitrary traction and displacement boundary conditions along its surface (Fig. 2b). The crack–inhomogeneity interaction is achieved by enforcing continuity of displacements along the interface and the stress jumps across the interface associated with the Gurtin and Murdoch model. Sections 2, 3 and 4 summarize the problem statement, governing equations, and numerical solution (with details provided in the Appendix). These are followed by illustrative examples in Sect. 5 and conclusions in Sect. 6.

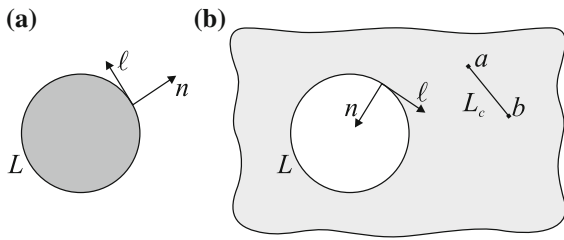


Fig. 2 **a** A circular disc. **b** A circular hole and a crack in an infinite plane

2 Problem statement

Consider (Fig. 1) the two-dimensional, plane strain problem of an infinite, isotropic elastic plane containing a perfectly bonded circular, isotropic elastic inhomogeneity interacting with a straight crack. The crack is arbitrarily located outside of the region defined by the inhomogeneity but does not intersect its boundary. The elastic properties of the inhomogeneity are quantified through the shear modulus μ_1 and Poisson’s ratios ν_1 while those of the plane are μ , and ν . Let R and L denote the radius and boundary of the inhomogeneity, and $z_0 = z_{01} + iz_{02}$ ($i = \sqrt{-1}$) the complex coordinate of its center. We suppose that $a = a_1 + ia_2$, $b = b_1 + ib_2$ are the complex coordinates of the beginning and end points of the crack with the boundary L_c . The interface between the inhomogeneity and the plane (matrix) is modeled as a material surface of vanishing thickness adhering to the bulk material without slipping. This surface is characterized by elastic constants (shear moduli μ_0 and Lamé parameters λ_0) and the residual surface tension σ_0 . The crack is either traction free or loaded with the prescribed pressure $\sigma^c(t)$, $t \in L_c$. The applied loading consists of a biaxial stress field at infinity ($\sigma_{xx}^\infty, \sigma_{yy}^\infty, \sigma_{xy}^\infty$). The distributions of stresses, displacements, and strains in the composite and the stress intensity factors at the crack tips are to be determined.

3 Governing equations

3.1 Boundary integral equations

The problem can be decomposed into two problems: the first is an elastic disc whose boundary is subjected to an unknown distributions of tractions and displacements and the second is an isotropic elastic plane containing a crack and a hole whose boundary is subjected to

unknown distributions of tractions and displacements. The two problems are interrelated through the Gurtin and Murdoch interface boundary conditions (Gurtin and Murdoch 1975).

Each elastostatic problem is formulated by using the direct boundary integral method, where all the elastic fields are represented in integral form via the Somigliana identities. The solution relies on the complex variables boundary element method described in Mogilevskaya and Linkov (1998), Linkov and Mogilevskaya (1998) and Linkov (2002).

The system of complex boundary integral equations for the problem includes the following:

- (i) *Somigliana’s traction identity at the boundary of the disc* (Linkov and Mogilevskaya 1998; Linkov 2002)

$$\begin{aligned}
 & 2\pi i \frac{\kappa_1 + 1}{4\mu_1} \sigma^{\text{inh}}(t) \\
 &= 2 \int_L \frac{u^{\text{inh}}(\tau)}{(\tau - t)^2} d\tau \\
 &\quad - \int_L u^{\text{inh}}(\tau) \frac{\partial}{\partial t} dK_1(\tau, t) \\
 &\quad - \int_L \overline{u^{\text{inh}}(\tau)} \frac{\partial}{\partial t} dK_2(\tau, t) \\
 &\quad + \frac{1 - \kappa_1}{2\mu_1} \int_L \frac{\sigma^{\text{inh}}(\tau)}{\tau - t} d\tau \\
 &\quad - \frac{\kappa_1}{2\mu_1} \int_L \sigma^{\text{inh}}(\tau) \frac{\partial}{\partial t} K_1(\tau, t) d\tau \\
 &\quad + \frac{1}{2\mu_1} \int_{L_k} \overline{\sigma^{\text{inh}}(\tau)} \frac{\partial}{\partial t} K_2(\tau, t) d\bar{\tau} \tag{1}
 \end{aligned}$$

where the superscript inh indicates the elastic fields for the inhomogeneity; $t = x + iy$ is complex coordinate of a point (x, y) on the contour L ; $\kappa_1 = 3 - 4\nu_1$; $\sigma^{\text{inh}}(t) = \sigma_n^{\text{inh}}(t) + i\sigma_\ell^{\text{inh}}(t)$ are the complex tractions at the boundary point t in a local coordinate system shown in Fig. 2a; $u^{\text{inh}}(\tau) = u_x^{\text{inh}}(\tau) + iu_y^{\text{inh}}(\tau)$ are the complex displacements at the boundary point τ in a global coordinate system; and a bar over a symbol denotes complex conjugation. The direction of integration is counterclockwise along boundary L .

The two kernels in Eq. (1) are:

$$K_1(\tau, t) = \ln \frac{\tau - t}{\bar{\tau} - \bar{t}}, \quad K_2(\tau, t) = \frac{\tau - t}{\bar{\tau} - \bar{t}} \quad (2)$$

- (ii) *Boundary integral equation at the boundary of the hole or crack* [obtained by summing Somigliana’s traction identity for the infinite plane with the hole with the complex hypersingular integral equation for the crack (Linkov and Mogilevskaya 1998; Linkov 2002)]

$$\begin{aligned} & 2 \int_L \frac{u^{\text{mat}}(\tau)}{(\tau - t)^2} d\tau \\ & - \int_L u^{\text{mat}}(\tau) \frac{\partial}{\partial t} dK_1(\tau, t) \\ & - \int_L u^{\text{mat}}(\tau) \frac{\partial}{\partial t} dK_2(\tau, t) \\ & + \frac{1 - \kappa}{2\mu} \int_L \frac{\sigma^{\text{mat}}(\tau)}{\tau - t} d\tau \\ & - \frac{\kappa}{2\mu} \int_L \sigma^{\text{mat}}(\tau) \frac{\partial}{\partial t} K_1(\tau, t) d\tau \\ & + \frac{1}{2\mu} \int_L \overline{\sigma^{\text{mat}}(\tau)} \frac{\partial}{\partial t} K_2(\tau, t) d\bar{\tau} \\ & + 2 \int_{L_c} \frac{\Delta u^c(\tau)}{(\tau - t)^2} d\tau \\ & - \int_{L_c} \Delta u^c(\tau) \frac{\partial}{\partial t} dK_1(\tau, t) \\ & - \int_{L_c} \overline{\Delta u^c(\tau)} \frac{\partial}{\partial t} dK_2(\tau, t) \\ & = 2\pi i \frac{1 + \kappa}{4\mu} \left[\alpha \sigma(t) \right. \\ & \left. + \sigma^\infty(t) \right], \quad t \in L \cup L_c \quad (3) \end{aligned}$$

where the superscript mat indicates the elastic fields for the matrix; $\kappa = 3 - 4\nu$; the complex displacements $u^{\text{mat}}(\tau)$ and the complex tractions $\sigma^{\text{mat}}(t)$ are defined similarly as those for the disc; $\Delta u^c(\tau) = \Delta u_x^c(\tau) + i \Delta u_y^c(\tau)$ is the complex displacement discontinuity at the point $\tau \in L_c$ in a global coordinate system, σ^∞ is a complex function that can be expressed via the stress at infinity as follows (Mogilevskaya and Crouch 2001):

$$\sigma^\infty(t) = - \left[\sigma_{xx}^\infty + \sigma_{yy}^\infty + \frac{d\bar{t}}{dt} \left(\sigma_{yy}^\infty - \sigma_{xx}^\infty - 2i\sigma_{xy}^\infty \right) \right]; \quad (4)$$

$d\bar{t}/dt = \exp(-2i\beta)$; β is the angle between the axis Ox and tangent at the point t ; and the coefficients α and the function $\sigma(t)$ are defined as follows:

$$\alpha = \begin{cases} 1 & t \in L \\ 2 & t \in L_c \end{cases}, \quad \sigma(t) = \begin{cases} \sigma^{\text{mat}}(t) & t \in L \\ \sigma^c(t) & t \in L_c \end{cases} \quad (5)$$

The direction of integration is clockwise for the boundary of the hole L and arbitrary for the boundary of the crack L_c . The unit normal \mathbf{n} points to the right of the direction of travel (i.e. inside the hole); the unit tangent ℓ is directed in the direction of integration (Fig. 2b).

- (iii) *Gurtin and Murdoch equations for the material surface* (Mogilevskaya et al. 2008). The real variables forms of the equations are:

- (a) Kinematic equations for the material surface. They include definitions of strain ε^{sur}

$$\varepsilon^{\text{sur}} = \frac{\partial u_\ell}{\partial s} + \frac{u_n}{R} \quad (6)$$

and rotation ω^{sur}

$$\omega^{\text{sur}} = -\frac{u_\ell}{R} + \frac{\partial u_n}{\partial s} \quad (7)$$

where u_ℓ and u_n are tangential and normal components of surface displacements in a local coordinate system shown in Fig. 2a and s is the arc length of the undeformed surface.

- (b) Constitutive equation for the surface

$$\sigma^{\text{sur}} = \sigma_0 + (2\mu_0 + \lambda_0)\varepsilon^{\text{sur}} \quad (8)$$

where σ^{sur} is a one-dimensional surface stress.

- (c) Continuity of displacements along the material surface

$$u_x^{\text{inh}} = u_x^{\text{mat}} = u_x, \quad u_y^{\text{inh}} = u_y^{\text{mat}} = u_y \quad (9)$$

- (d) Surface equilibrium conditions

$$\begin{aligned} \sigma_\ell^{\text{inh}} - \sigma_\ell^{\text{mat}} &= \frac{\partial \sigma^{\text{sur}}}{\partial s} + \frac{\sigma_0 \omega^{\text{sur}}}{R} \\ \sigma_n^{\text{inh}} - \sigma_n^{\text{mat}} &= -\frac{1}{R} \sigma^{\text{sur}} + \frac{\sigma_0 \partial \omega^{\text{sur}}}{\partial s} \end{aligned} \quad (10)$$

Often times only the first terms on the right hand sides of the above equations are retained. However, in many situations (e.g. large surface tension σ_0 , small radius R of the inhomogeneity) the second terms have been shown (Mogilevskaya et al. 2008) to have significant effects. The presence of those terms reflects the fact that the true surface stress is tangent to the surface deformed configuration, while Eqs. (10) are written in its initial configuration. Relative to that initial configuration, the stress tensor has a tangent component described by Eq. (8) and a normal component of magnitude $\sigma_0\omega^{\text{sur}}$. The second terms of the right-hand side of Eqs. (10) represent contributions of that normal component to the surface equilibrium conditions.

It was shown in Mogilevskaya et al. (2008) that the Gurtin and Murdoch equations for the material surface can be expressed in the following complex forms:

$$\begin{aligned}
 u^{\text{inh}}(\tau) &= u^{\text{mat}}(\tau) = u(\tau) & (11) \\
 \sigma_n^{\text{inh}}(\tau) - \sigma_n^{\text{mat}}(\tau) &= -\frac{1}{R} \left[\sigma_0 + (2\mu_0 + \lambda_0) \text{Re} \frac{\partial u(\tau)}{\partial \tau} \right] \\
 &\quad - \sigma_0 \text{Re} \left[\frac{\partial^2 u(\tau)}{\partial \tau^2} g^{-1}(\tau) \right] \\
 \sigma_\ell^{\text{inh}}(\tau) - \sigma_\ell^{\text{mat}}(\tau) &= -(2\mu_0 + \lambda_0) \text{Im} \left[\frac{\partial^2 u(\tau)}{\partial \tau^2} g^{-1}(\tau) \right] \\
 &\quad - \frac{\sigma_0}{R} \text{Im} \frac{\partial u(\tau)}{\partial \tau}
 \end{aligned}$$

where

$$g(\tau) = \frac{R}{\tau - z_0} \tag{12}$$

It can be seen from Eqs.(10) and (7) that when $R \rightarrow \infty$, the jump in the tangential component of tractions is entirely due to surface elasticity; while the jump in the normal component is entirely due to surface tension. In the simplified versions of the Gurtin and Murdoch equations (employed in most of the publications on the topic) the term ω^{sur} is neglected and thus the jump in normal component vanishes when $R \rightarrow \infty$.

3.2 Evaluation of the elastic fields in the composite system and the stress intensity factors at the crack tips

The displacements and stresses at any point in the composite can be expressed in terms of two complex Kolosov–Muschelishvili potentials $\varphi(z)$ and $\psi(z)$ by

using well-known Kolosov–Muschelishvili formulae (Muskhelishvili 1959). After the solution of the system (1), (3), and (11), the expressions for the potentials can be written in terms of integrals of known boundary tractions and stresses at infinity as follows:

- (a) potentials for the circular disc (Linkov and Mogilevskaya 1998; Linkov 2002)

$$\begin{aligned}
 \varphi(z) &= -\frac{1}{2\pi i(\kappa_1 + 1)} \int_L \sigma^{\text{inh}}(\tau) \ln(\tau - z) d\tau \\
 &\quad + \frac{\mu_1}{\pi i(\kappa_1 + 1)} \int_L \frac{u(\tau)}{\tau - z} d\tau & (13) \\
 \psi(z) &= -\frac{1}{2\pi i(\kappa_1 + 1)} \left[\int_L \sigma^{\text{inh}}(\tau) \frac{\bar{\tau}}{\tau - z} d\tau \right. \\
 &\quad \left. + \kappa_1 \int_L \bar{\sigma}^{\text{inh}}(\tau) \ln(\tau - z) d\bar{\tau} \right] \\
 &\quad + \frac{\mu_1}{\pi i(\kappa_1 + 1)} \left[\int_L u(\tau) d \frac{\bar{\tau}}{\tau - z} \right. \\
 &\quad \left. - \int_L \frac{\bar{u}(\tau)}{\tau - z} d\tau \right]
 \end{aligned}$$

- (b) potentials for the bulk material of the matrix (Linkov and Mogilevskaya 1998; Linkov 2002)

$$\begin{aligned}
 \varphi(z) &= \varphi_h(z) + \varphi_c(z) + \varphi^\infty(z) \\
 \psi(z) &= \psi_h(z) + \psi_c(z) + \psi^\infty(z)
 \end{aligned}$$

where

$$\begin{aligned}
 \varphi_h(z) &= \frac{1}{2\pi i(\kappa + 1)} \left[-\int_L \sigma^{\text{mat}}(\tau) \ln(\tau - z) d\tau \right. \\
 &\quad \left. + 2\mu \int_L \frac{u(\tau)}{\tau - z} d\tau \right] & (14) \\
 \psi_h(z) &= \frac{1}{2\pi i(\kappa + 1)} \left\{ -\left[\int_L \sigma^{\text{mat}}(\tau) \frac{\bar{\tau}}{\tau - z} d\tau \right. \right. \\
 &\quad \left. \left. + \kappa \int_L \bar{\sigma}^{\text{mat}}(\tau) \ln(\tau - z) d\bar{\tau} \right] \right\}
 \end{aligned}$$

$$\begin{aligned}
 & \left. \begin{aligned}
 & +2\mu \left[\int_L u(\tau) d\frac{\bar{\tau}}{\tau-z} \right. \\
 & \left. - \int_L \frac{\bar{u}(\tau)}{\tau-z} d\tau \right] \Bigg\} \\
 \varphi_c(z) = & \frac{1}{2\pi i(\kappa+1)} \left[- \int_{L_c} \sigma^c(\tau) \ln(\tau-z) d\tau \right. \\
 & \left. + 2\mu \int_{L_c} \frac{\Delta u^c(\tau)}{\tau-z} d\tau \right] \quad (15) \\
 \psi_c(z) = & \frac{1}{2\pi i(\kappa+1)} \left\{ - \left[\int_{L_c} \sigma^c(\tau) \frac{\bar{\tau}}{\tau-z} d\tau \right. \right. \\
 & \left. \left. + \kappa \int_{L_c} \bar{\sigma}^c(\tau) \ln(\tau-z) d\bar{\tau} \right] \right. \\
 & \left. + 2\mu \left[\int_{L_c} \Delta u^c(\tau) d\frac{\bar{\tau}}{\tau-z} \right. \right. \\
 & \left. \left. - \int_{L_c} \frac{\overline{\Delta u^c(\tau)}}{\tau-z} d\tau \right] \right\}
 \end{aligned}$$

and where the potentials at infinity are as follows:

$$\begin{aligned}
 \varphi^\infty(z) &= \frac{\sigma_{xx}^\infty + \sigma_{yy}^\infty}{4} z \\
 \psi^\infty(z) &= \frac{\sigma_{yy}^\infty - \sigma_{xx}^\infty + 2i\sigma_{xy}^\infty}{2} z \quad (16)
 \end{aligned}$$

The displacements are defined up to some additional terms, which can be found by a procedure similar to the one described in Mogilevskaya et al. (2008).

The stress intensity factors at the tips of the crack can be calculated from the following expressions (Mogilevskaya 1996):

$$\begin{aligned}
 & (K_1 - iK_2)_a \\
 &= -\frac{\sqrt{2\pi}\mu i}{\kappa+1} \exp(-i\theta_1/2) \lim_{\tau \rightarrow a} \left(\frac{\Delta u}{\sqrt{\tau-a}} \right) \\
 & (K_1 - iK_2)_b \\
 &= -\frac{\sqrt{2\pi}\mu i}{\kappa+1} \exp(-i\theta_2/2) \lim_{\tau \rightarrow b} \left(\frac{\Delta u}{\sqrt{b-\tau}} \right) \quad (17)
 \end{aligned}$$

where θ_1 (θ_2) is the angle between the axis Ox and the tangent to the tip a (b).

4 Numerical solution

4.1 Circular disc

We expand the unknown tractions $\sigma^{inh}(\tau)$ and the displacements $u(\tau)$ at the boundary of the disc into complex Fourier series of the forms

$$\begin{aligned}
 \sigma^{inh}(\tau) &= \sum_{m=1}^\infty B_{-m}^{inh} g^m(\tau) \\
 &+ \sum_{m=0}^\infty B_m^{inh} g^{-m}(\tau), \quad \tau \in L \quad (18)
 \end{aligned}$$

$$\begin{aligned}
 u^{inh}(\tau) &= u(\tau) \\
 &= \sum_{m=1}^\infty A_{-m} g^m(\tau) \\
 &+ \sum_{m=0}^\infty A_m g^{-m}(\tau), \quad \tau \in L \quad (19)
 \end{aligned}$$

where $g(\tau)$ is defined by Eq. (12). The complex coefficients in series (18) and (19) are unknown. After substituting expressions (18) and (19) into Eq. (1), evaluating all integrals analytically and using the properties of complex Fourier series, the coefficients for the tractions (B_{-m}^{inh} , B_m^{inh}) can be expressed in terms of those for the displacements (A_{-m} , A_m) (see Mogilevskaya et al. 2008 for more details).

4.2 Infinite plane containing the hole and the crack

The complex Fourier series for the unknown tractions $\sigma^{mat}(\tau)$ at the boundary of the hole can be written as follows

$$\begin{aligned}
 \sigma^{mat}(\tau) &= \sum_{m=1}^\infty B_{-m}^{mat} g^m(\tau) \\
 &+ \sum_{m=0}^\infty B_m^{mat} g^{-m}(\tau), \quad \tau \in L \quad (20)
 \end{aligned}$$

The displacements $u(\tau)$ at the same boundary can be represented by series (19) due to condition (11).

To represent the unknown displacement discontinuities at the boundary of the cracks we first map the crack segment $[a, b]$ onto the segment $[-1, 1]$ as follows:

$$s = \frac{2\tau - a - b}{b - a}, \quad \tau \in L_c$$

The displacement discontinuity distribution $\Delta u^c(s)$ along the segment $[-1, 1]$ is then approximated by series of Chebyshev polynomials multiplied by a weight function $\sqrt{1 - s^2}$

$$\Delta u^c(s) = \sqrt{1 - s^2} \sum_{n=0}^{\infty} d_n U_n(s) \tag{21}$$

where $U_n(s)$ is the Chebyshev polynomial of the second kind defined as

$$U_n(s) = \frac{\sin[(n + 1) \arccos s]}{\sin(\arccos s)} \tag{22}$$

The weight function involved in Eq.(21) is introduced to take into account the correct tip asymptotics. The complex coefficients in series (20) and (21) are unknown.

Using relations (19) and (11), we can express the coefficients for the tractions (B_{-m}^{mat}, B_m^{mat}) in terms of those for the displacements (A_{-m}, A_m) (see Mogilevskaya et al. (2008) for more details). Thus, one can rewrite Eq.(3) in terms of unknown coefficients for the displacements and displacement discontinuities only. After these coefficients are determined, the tractions and displacements at the boundary of the inhomogeneity and the displacement discontinuities at the boundary of the crack can be found. The procedure of determining the unknown coefficients for the displacements and displacement discontinuities is outlined in the Appendix 1.

The displacements, stresses, strains and stress intensity factors in the system can be evaluated as explained in Appendix 2.

5 Examples

5.1 Parametric studies

The number of the parameters that govern the problem is rather large and, in this section, we restrict our studies to the cases we deem the most interesting from the point of view of influence of the surface effects on the stress intensity factors at the crack tips. Thus we consider the problem depicted in Fig.3. We also assume that the Poisson’s ratios of the matrix and inhomogeneity are fixed: $\nu = 0.35, \nu_1 = 0.3$ ($\nu_1 = 0$ for a cavity) and that the crack is traction-free. Using the following scaling for the unknowns

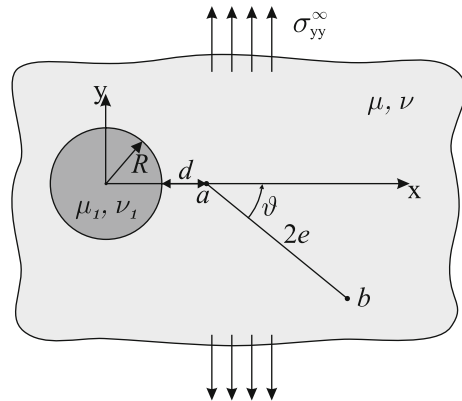


Fig. 3 Example problem

$$\sigma/\mu, u/R, \Delta u/\ell \tag{23}$$

one can conclude from the analysis of Eqs.(29) and (31) in Appendix 1 (taking into account that $\eta/\mu = \lambda/2, \eta^{(1)}/\mu = (\lambda + \chi)/2, \eta^{(2)}/\mu = (\lambda - \chi)/2$) that the problem is governed by the following dimensionless parameters

$$\begin{aligned} \lambda &= (2\mu_0 + \lambda_0)/(2\mu R), \\ \chi &= \sigma_0/(2\mu R), \ell/R, \mu_1/\mu, d/R, \vartheta, \\ \zeta &= \sigma_{yy}^\infty/(2\mu) \end{aligned} \tag{24}$$

Below we study the influence of these parameters on the stress intensity factors at the crack tip located closest to the inhomogeneity. All examples, with the exception of the one presented in Sect. 5.1.2.6, assume that $\vartheta = 0^\circ$, for which the mode-I stress intensity factor is likely to be the largest. In all the numerical simulations reported we take the computational tolerance parameters δ and δ_1 to be $\delta = 0.005, \delta_1 = 0.01$ (Appendix 1). For the illustration purposes, in some examples, the range of values for parameters λ and χ was chosen significantly larger than the available data characterizing nano-composites reported in the literature (see e.g. Gurtin and Murdoch (1978); Miller and Shenoy (2000); Sharma and Ganti (2002, 2004); Yang (2004); Duan et al. (2005c, 2006); He and Li (2006); Chen et al. (2007)).

5.1.1 Qualitative evaluation of shielding and anti-shielding related to the parameters λ (surface elasticity) and χ (surface tension)

First we consider an isolated cavity with no crack ($\ell/R = 0, \vartheta = 0^\circ, \mu_1/\mu = 0$) and investigate the

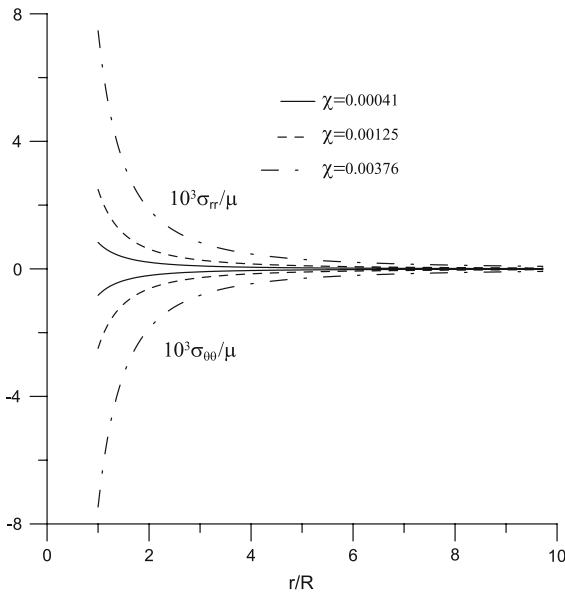


Fig. 4 Variation of the normalized stresses along the axis Ox with the parameter r/R ($\lambda = 0, \ell/R = 0, \mu_1/\mu = 0, \zeta = 0.0$)

influence of the surface tension and surface elasticity on the distribution of σ_{rr}/μ and/or $\sigma_{\theta\theta}/\mu$. This reference example, which can be solved in elementary fashion, will facilitate the better understanding of the subsequent results related to the shielding/antishielding effects.

To study the influence of the parameter χ on the stresses we assume that $\lambda = 0$ and $\zeta = 0$. It can be seen from Fig. 4 that, as expected, the surface tension produces tensile radial stresses σ_{rr}/μ and compressive hoop stresses $\sigma_{\theta\theta}/\mu$, both rapidly decreasing with the distance from the cavity. This stress distribution is axisymmetric, thus components of σ_{xx}, σ_{yy} and σ_{xy} relative to a coordinate system xy are invariant with respect to its rotation.

Figure 5a shows the contours of normalized stress component σ_{yy}/μ and provides insight into whether the stress intensity factors will be reduced or amplified when the crack is located at a particular location perpendicular to y axis. This figure, appropriately rotated, can provide qualitative information about shielding or antishielding for an arbitrary located crack. For example, for a crack AB shown on Fig. 5b, the coordinate axes and the boundaries separating the zones of shielding and antishielding (dashed lines) are rotated so as to make the x' axis parallel to the crack. For this particular location of the crack, the surface tension is likely to

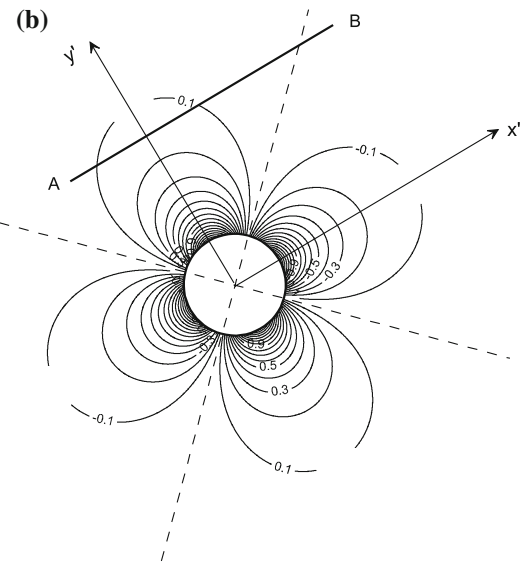
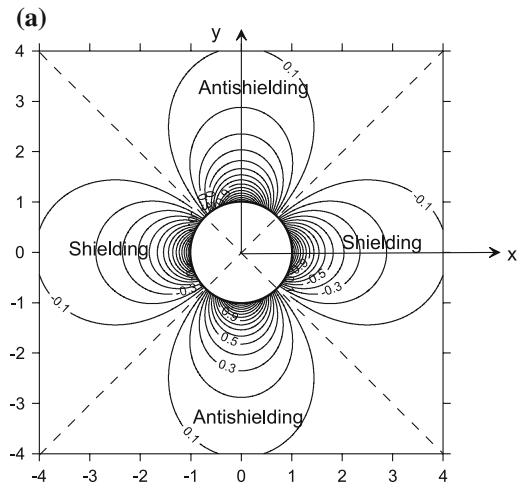


Fig. 5 **a** Contours of $10^3\sigma_{yy}/\mu$ around the cavity ($\lambda = 0, \chi = 0.00083, \ell/R = 0, \mu_1/\mu = 0, \zeta = 0.0$), **b** contours rotated to determine shielding/antishielding for a particular crack AB

amplify the stress intensity factor at tip A and reduce it at tip B .

The above analysis is only qualitative, since the presence of the crack disturbs the stress field produced by the surface tension. Nonetheless, the analysis provides a general view of the interaction between the crack and the cavity with the surface tension. This view is confirmed in several examples presented in the following subsections.

A qualitative illustration of how surface elasticity alone ($\chi = 0, \lambda \neq 0$) affects crack tip stress

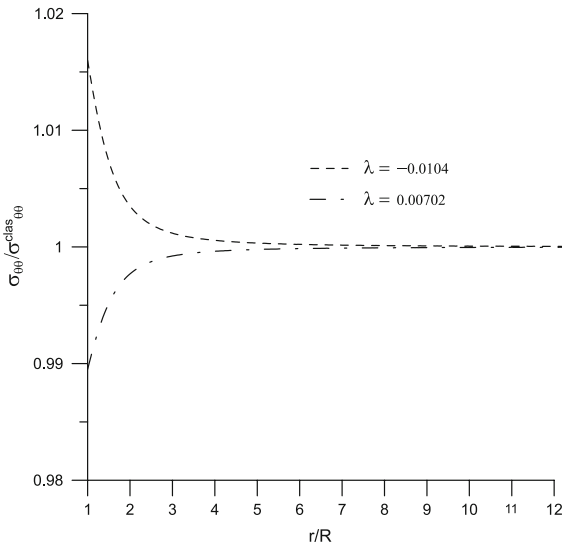
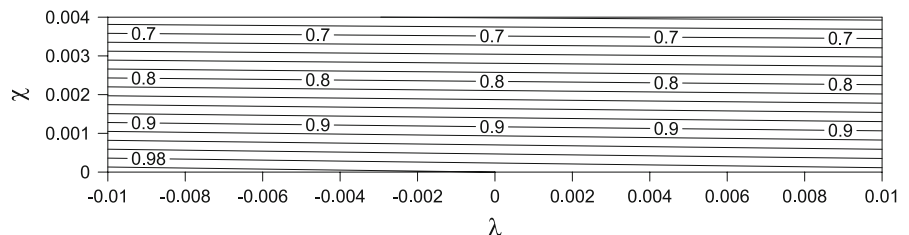


Fig. 6 Variation of the normalized stresses along the axis Ox with the parameter r/R ($\chi = 0, \ell/R = 0, \mu_1/\mu = 0, \zeta = 0.0014$)

intensity factors requires a specific load. Consequently, in Fig. 6 we present only a normalized distribution of hoop stress $\sigma_{\theta\theta}/\sigma_{\theta\theta}^{clas}$ (where $\sigma_{\theta\theta}^{clas}$ is the hoop stress for the corresponding classical problem without surface effects) along the radial direction perpendicular to the load $\zeta = 0.0014$. For the selected two values of surface elasticity parameters, the influence of surface elasticity is insignificant and localized. For a crack along that specific radial direction a positive (negative) value of the surface elasticity parameter will be associated with shielding (antishielding). Although this is only a specific situation, it is arguably, very representative. Figure 6 indicates that, in absence of surface tension, the interaction between the crack and the cavity will not be significantly affected by surface elasticity, and if so than only when the parameter d/R is very small. The influence of surface elasticity and surface tension on the stress intensity factor at crack tip b will generally be small, particularly for longer cracks.

Fig. 7 Variation of the normalized stress intensity factor $F_1(a)$ with the parameters λ and χ ($d/R = 0.2, \ell/R = 10, \vartheta = 0^\circ, \mu_1/\mu = 0, \zeta = 0.0014$)



5.1.2 Quantitative evaluation of crack–cavity interaction

We now proceed to study the interaction between the crack and the cavity in a more precise manner.

5.1.2.1. Dependence of stress intensity factor on surface parameters

We consider the following parameters: $d/R = 0.2, \ell/R = 10, \vartheta = 0^\circ, \mu_1/\mu = 0, \zeta = 0.0014$. Figure 7 shows the contours of the normalized stress intensity factor $F_1(a)$ at the crack tip a as the function of the parameters λ and χ ($F_1(a) = K_1(a)/K_1^{clas}(a)$ where $K_1^{clas}(a)$ is the stress intensity factor of the corresponding classical problem in which $\lambda = 0, \chi = 0$). In accord with the observation in the preceding subsection, one can conclude that for the considered configuration of the crack, an increase in surface tension results in a decrease in the normalized stress intensity factors, and that the influence of surface elasticity is insignificant. Even though the contours presented in Fig. 7 may be perceived as straight lines, careful examination of the figures does reveal that dependence of $F_1(a)$ on the parameters λ and χ is, in fact, slightly non-linear.

5.1.2.2. Influence of the parameters χ (normalized surface tension) and ζ (normalized load)

The form of the governing equations, containing surface tension σ_0 and the load σ_{yy}^∞ , does not allow for the superposition with respect to the load. This example is meant to present the quantitative representation of that feature. We choose the following parameters $d/R = 0.2, \ell/R = 10, \vartheta = 0^\circ, \mu_1/\mu = 0, \lambda = 0$. Figure 8 shows the contours of the normalized stress intensity factor $F_1(a)$ at the crack tip a as the function of the parameters χ and ζ . One can see from the figure that the dependence of $F_1(a)$ on the surface tension and load

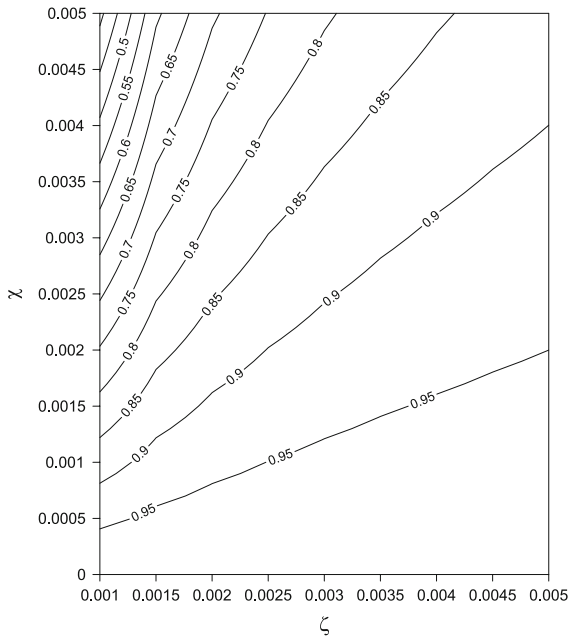


Fig. 8 Variation of the normalized stress intensity factor $F_1(a)$ with the parameters ζ and χ ($d/R = 0.2, \ell/R = 10, \vartheta = 0^\circ, \mu_1/\mu = 0, \lambda = 0$)

is strongly non-linear, particularly for smaller loads and larger surface tension. We emphasize that it happens even though in this example we have neglected surface elasticity. Consequently, this non-linearity is entirely due to the presence of ω^{sur} in Eq. (10). Although present in the original Gurtin and Murdoch model, this term has been neglected in virtually all publications dealing with the effects of surface tension. This is another example illustrating important influence of ω^{sur} , which persists even if $R \rightarrow \infty$.

5.1.2.3. Influence of the relative crack length

We take the following parameters $d/R = 0.04, \vartheta = 0^\circ, \mu_1/\mu = 0, \sigma_{yy}^\infty/(2\mu) = 0.0014$ and choose the three sets of surface/interface parameters (1) $\lambda = \chi = 0$; (2) $\lambda = -0.0052, \chi = 0$; (3) $\lambda = 0, \chi = 0.00083$. Figure 9 shows the results for the normalized stress intensity factor $F_1(a)$ at the crack tip a as the function of the parameter ℓ/R . It is observed that surface elasticity has insignificant effect on the normalized stress intensity factor $F_1(a)$. The effect of the surface tension on $F_1(a)$ is more pronounced. The effects of both the surface elasticity and surface tension on $F_1(b)$ (not shown

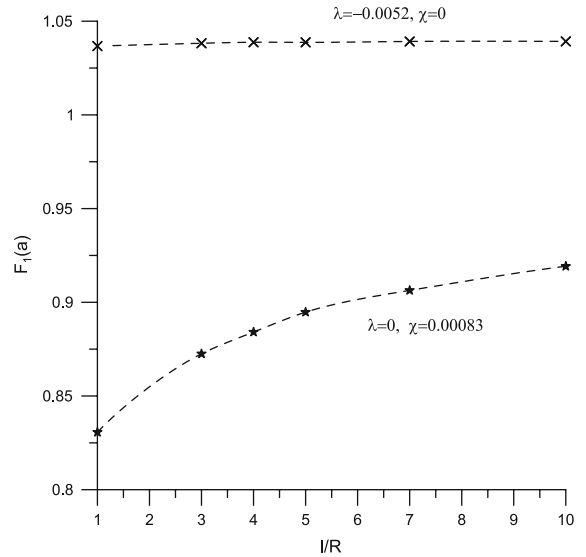


Fig. 9 Variation of the normalized stress intensity factor $F_1(a)$ with the parameter ℓ/R ($d/R = 0.04, \vartheta = 0^\circ, \mu_1/\mu = 0, \zeta = 0.0014$)

here) are less pronounced and they rapidly decrease with increasing ℓ/R .

5.1.2.4. Influence of the contrast in elastic properties of the bulk material and inhomogeneity

Consider the problem governed by the following parameters: $d/R = 0.04, \ell/R = 10, \sigma_{yy}^\infty/(2\mu) = 0.0014$ and choose the three sets of surface/interface parameters (1) $\lambda = \chi = 0$; (2) $\lambda = -0.0052, \chi = 0$; (3) $\lambda = 0, \chi = 0.00083$. We assume the inclination angle $\vartheta = 0^\circ$ and emphasize that Poisson's ratios of the matrix and inhomogeneity are different, $\nu = 0.35, \nu_1 = 0.3$. Figure 10 shows the results for the normalized stress intensity factor $F_1(a)$ at the crack tip a as the function of the parameter μ_1/μ . The effects of both surface elasticity and surface tension decrease as the stiffness of inhomogeneity increases. These trends are natural in view of the fact that for a rigid inhomogeneity surface/interface effects play no role.

5.1.2.5. Influence of the relative separation parameter d/R

We take the following parameters $\ell/R = 10, \vartheta = 0^\circ, \mu_1/\mu = 0, \sigma_{yy}^\infty/(2\mu) = 0.0014$ and choose the surface/interface parameters to be the ones described

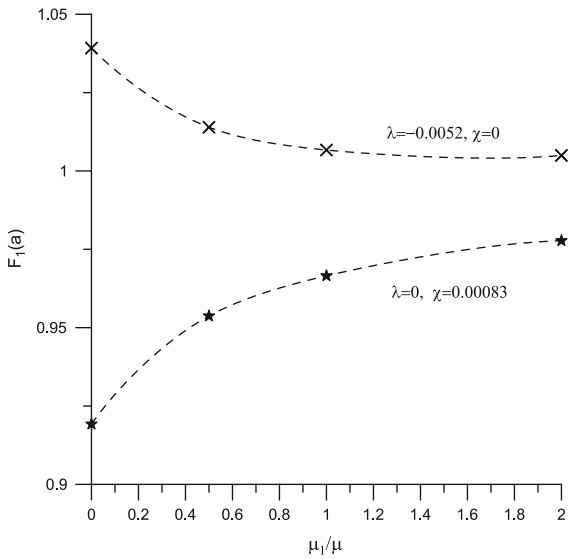


Fig. 10 Variation of the normalized stress intensity factor $F_1(a)$ with the contrast μ_1/μ ($d/R = 0.04, \ell/R = 10, \vartheta = 0^\circ, \zeta = 0.0014$)

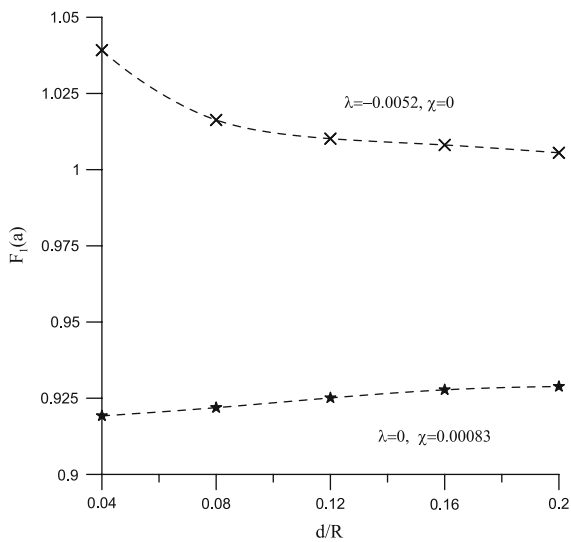


Fig. 11 Variation of the normalized stress intensity factor $F_1(a)$ with the parameter d/R ($\mu_1/\mu = 0, \ell/R = 10, \vartheta = 0^\circ, \zeta = 0.0014$)

in Sect. 5.1.2.3. Figures 11 shows the results for the normalized stress intensity factor $F_1(a)$ at the crack tip a as the function of the parameter d/R . It can be seen from this figure that for the data we have considered, the surface/interface effects are of the order of 5–10% along the entire range of values d/R . The effects due

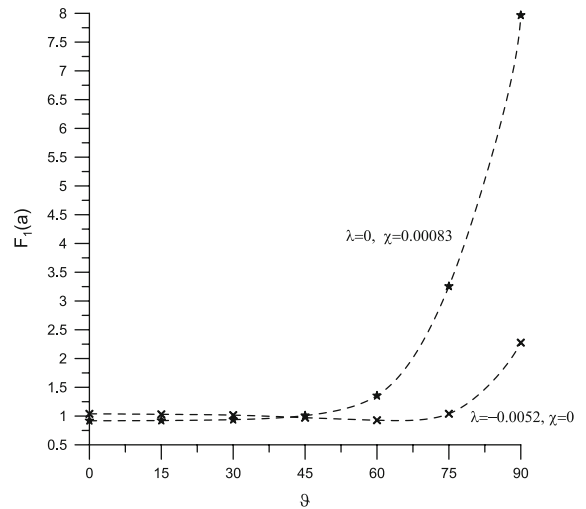


Fig. 12 Variation of the normalized stress intensity factor $F_1(a)$ with the inclination angle ϑ ($d/R = 0.04, \ell/R = 10, \mu_1/\mu = 0, \zeta = 0.0014$)

to surface tension are more profound than the ones due to surface elasticity. As expected both effects diminish with the increase in the relative separation parameter.

5.1.2.6. Influence of the inclination angle ϑ

We take the following parameters $d/R = 0.04, \ell/R = 10, \mu_1/\mu = 0, \sigma_{yy}^\infty/(2\mu) = 0.0014$ and choose the surface/interface parameters to be the ones described in Sect. 5.1.2.3. Qualitative observations of Sect. 5.1.1 suggest that with the rotation of the crack its stationary tip initially shielded by the surface tension (approximately for $0 \leq \vartheta < 45^\circ$) ends up experiencing antishielding (approximately for $45^\circ < \vartheta \leq 90^\circ$). Similar qualitative observations of Sect. 5.1.1 related to surface elasticity suggest it produces less pronounced shielding/antishielding effects. This is reflected in Fig. 12, which shows the results for the normalized stress intensity factor $F_1(a)$ at the crack tip a as the functions of the parameter ϑ . One can see from Fig. 12 that surface tension has a pronounced influence on the normalized stress intensity factor $F_1(a)$, except for a neighborhood of $\vartheta = 45^\circ$. This angle approximately defines the position of the crack at which the influence of the surface tension changes from shielding to anti-shielding. As can be seen from Fig. 12 for $\vartheta = 90^\circ$, there is about eight-fold amplification of $F_1(a)$. However, this

Fig. 13 Variation of the normalized stress intensity factor $F_1(a)$ with the parameters λ and χ ($d/R = 0.2, \ell/R = 10, \vartheta = 90^\circ, \mu_1/\mu = 0, \zeta = 0, \sigma_{xx}^\infty/(2\mu) = 0.0014$)

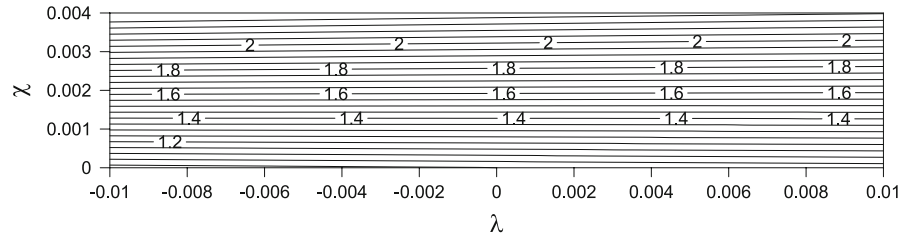
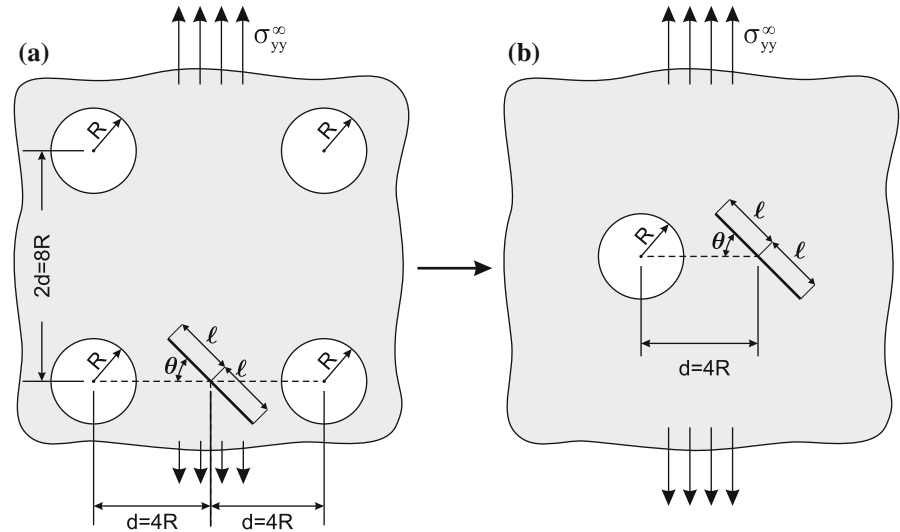


Fig. 14 **a** The problem used to investigate flaw tolerance of porous material. **b** Simplified model of the problem



picture may be somewhat misleading as the absolute value of $K_1(a)/(\sqrt{\pi\ell}\sigma_{yy}^\infty) = 0.46$ for $\vartheta = 90^\circ$ is still significantly smaller than the absolute value of $K_1(a)/(\sqrt{\pi\ell}\sigma_{yy}^\infty) = 2.32$ for $\vartheta = 0^\circ$.

For the case $\vartheta = 90^\circ$, the far-field load assumed in the analysis is parallel to the crack. Classical solution (without surface effects) for this case yields very small $K_1(a)$. The contribution of surface tension in this case is dominant, which explains the large amplification factor. To gain additional insight, we consider the same case of $\vartheta = 90^\circ$ and applied the load σ_{xx}^∞ instead of σ_{yy}^∞ . Figure 13 shows the contours of the normalized stress intensity factor $F_1(a)$ as the function of the parameters λ and χ . As can be seen from this figure the qualitative dependence of $F_1(a)$ on λ and χ is similar to the one presented in Fig. 7. The difference is that now amplification takes place rather than shielding and its magnitude is significantly larger than that of Fig. 7. Still the absolute value of $K_1(a)$ in this case is smaller than that $K_1(a)$ for $\vartheta = 0^\circ$ (discussed in the previous paragraph).

5.2 Effects of surface tension on flaw tolerance in porous materials

The issue we would like to illustrate here is a very complex one and we provide only a very approximate qualitative analysis of an idealized problem. We assume that we have a perforated plate with circular cavities of radius R , distributed on a perfect square grid with dimension $2d = 8R$ (for example). We further assume that the load is parallel to one side of the grid and that a crack develops that is centered along the line perpendicular to the load and connecting two neighboring cavities, Fig. 14a. The half-length ℓ of the crack may vary in the interval $(R, 2.96R)$ and its orientation ϑ in the interval $(-0.5\pi, 0.5\pi)$, and every value of ℓ and ϑ is equally likely (uniform probability distribution).

The question we ask is how the expected value of the energy release rate G is affected by surface tension. The answer to this question can be gleaned from the value of the ratio

$$\rho = \frac{G}{G^{\text{clas}}}$$

with

$$G = \frac{1-\nu}{2\mu} \int_{-\pi/2}^{\pi/2} \int_R [(K_1(a))^2 + (K_2(a))^2] d\ell d\vartheta$$

$$G^{\text{clas}} = \frac{1-\nu}{2\mu} \int_{-\pi/2}^{\pi/2} \int_R [(K_1^{\text{clas}}(a))^2 + (K_2^{\text{clas}}(a))^2] d\ell d\vartheta$$

where the superscript “clas”, relates to the values associated with the corresponding classical problem in which $\lambda = 0, \chi = 0$. Shielding (antishielding) is associated with $\rho < 1$ ($\rho > 1$).

To analyze the problem shown in Fig. 14a we assume that distance $d = 4R$ is large enough to neglect interactions between the cavities, and that the analysis can be performed using the model shown in Fig. 14b. For the data assumed in the analysis ($\lambda = 0, \chi = 0.00083, \mu_1/\mu = 0, \sigma_{yy}^\infty/(2\mu) = 0.0014$) we obtain $\rho = 0.925$, which implies that surface tension is likely to increase slightly the flaw tolerance of the porous material.

6 Conclusions

In this paper, for the first time, we investigated the problem of the interaction between a circular inhomogeneity with surface/interface effects and a straight crack. Numerical examples are presented to quantify and discuss the main features of that interaction. Those examples were solved using an effective numerical technique that allows one to obtain accurate information about the elastic fields inside and outside of the inhomogeneity.

The obtained results, reported in Sect. 5, reveal several characteristics of the problem. It has been shown that, for some values of the problem parameters, surface tension may significantly change the stress intensity factors at the tips of the crack. However, the effects of surface elasticity are rather insignificant. We have also documented that ω^{sur} causes the stress intensity factors to depend non-linearly on surface tension. This feature, as well as the lack of superposition with respect to the

load, is one of the main characteristics of problems with the surface/interface effects.

While we restricted ourselves to the problem of a single crack and a single inhomogeneity, the technique employed in this work is applicable to problems with multiple inhomogeneities and cracks. Such scenario would be more typical for practical applications, particularly in the analysis of nano-composite materials. Incorporation of surface tension and surface elasticity in crack model is another direction for possible extension of the method.

Appendix 1

System of complex equations

The system of equations that contains the unknown coefficients for the displacements and displacement discontinuities only has the following form:

(i) $t \in L$

$$4\text{Re} \frac{A_1}{R} \left[\frac{\mu_1/\mu}{\kappa_1 - 1} + \frac{\eta}{\mu} + \frac{1}{2} \right]$$

$$+ \sum_{m=1}^{\infty} m \frac{A_{-m}}{R} g^{m+1}(t)$$

$$\left[1 + \kappa \left(\frac{\mu_1}{\mu} + m \frac{\eta^{(1)}}{\mu} \right) \right]$$

$$+ \sum_{m=1}^{\infty} (m+1) \frac{A_{(m+1)}}{R} g^{-m}(t)$$

$$\left[1 + \frac{\mu_1/\mu}{\kappa_1} + (m+1) \frac{\eta^{(1)}}{\mu} \right]$$

$$- \sum_{m=2}^{\infty} (m-1)(m+1) \frac{\eta^{(2)}}{\mu} \frac{\bar{A}_{-(m-1)}}{R} g^{-m}(t)$$

$$- \sum_{m=2}^{\infty} (m-1)(m+1) \kappa \frac{\eta^{(2)}}{\mu} \frac{\bar{A}_{(m+1)}}{R} g^m(t)$$

$$+ \frac{i}{\pi} \sum_{n=0}^{\infty} \frac{d_n}{b-a} \left[I_1(s_t, n) - \gamma_1 g^2(t) \overline{I_1(s_t, n)} \right]$$

$$- \frac{i}{\pi} \sum_{n=0}^{\infty} \frac{\bar{d}_n}{\bar{b}-\bar{a}} \left\{ \left[1 + \gamma_1 g^2(t) \right] \overline{I_1(s_t, n)} \right.$$

$$\left. + 2\gamma_1 g^2(t) (\bar{s}_t - s_t) \overline{I_2(s_t, n)} \right\}$$

$$= \frac{\kappa + 1}{4\mu} \left[\sigma_{xx}^\infty + \sigma_{yy}^\infty - g^2(t) \left(\sigma_{yy}^\infty - \sigma_{xx}^\infty - 2i\sigma_{xy}^\infty \right) \right] - \frac{\sigma_0}{\mu R} \quad (25)$$

(i) $t \in L_c$

$$\begin{aligned} & \frac{2}{\gamma_1} \overline{g^2(t)} \operatorname{Re} \frac{A_1}{R} \\ & \left[1 - (\kappa - 1) \left(\frac{\mu_1/\mu}{\kappa_1 - 1} + \frac{\eta}{\mu} \right) \right] \\ & - \sum_{m=1}^\infty m \frac{A_{-m}}{R} \overline{g^{m+1}(t)} \\ & \left[1 - \frac{\mu_1}{\mu} - m \frac{\eta^{(1)}}{\mu} \right] \\ & + \frac{1}{\gamma_1} \sum_{m=1}^\infty (m + 1) \frac{A_{(m+1)}}{R} \overline{g^m(t)} \\ & \times \left\{ \left[1 - \frac{\kappa}{\kappa_1} \frac{\mu_1}{\mu} - \kappa (m + 1) \frac{\eta^{(1)}}{\mu} \right. \right. \\ & \left. \left. - (m - 1)(m + 1) \frac{\eta^{(2)}}{\mu} \right] \overline{g^2(t)} \right. \\ & \left. + (m - 1) \frac{\eta^{(2)}}{\mu} \left[-\gamma_1 + m g^{-1}(t) \overline{g(t)} \right] \right\} \\ & - \frac{1}{\gamma_1} \sum_{m=1}^\infty m \frac{\overline{A_{-m}}}{R} \overline{g^{m+1}(t)} \\ & \times \left\{ \left[\gamma_1 - (m + 1) g^{-1}(t) \overline{g(t)} \right. \right. \\ & \left. \left. + (m + 2) \overline{g^2(t)} \right] \left[1 - \frac{\mu_1}{\mu} - m \frac{\eta^{(1)}}{\mu} \right] \right. \\ & \left. + \kappa (m + 2) \frac{\eta^{(2)}}{\mu} \overline{g^2(t)} \right\} \\ & - \sum_{m=2}^\infty (m - 1)(m + 1) \\ & \times \frac{\eta^{(2)}}{\mu} \frac{\overline{A_{(m+1)}}}{R} \overline{g^m(t)} \\ & + 2i \sum_{n=0}^\infty \frac{d_n}{b - a} (n + 1) U_n(s_t) \\ & = \frac{\kappa + 1}{4\mu} \left[2\sigma^c(t) - \left(\sigma_{xx}^\infty + \sigma_{yy}^\infty \right) \right. \\ & \left. - \frac{1}{\gamma_1} \left(\sigma_{yy}^\infty - \sigma_{xx}^\infty - 2i\sigma_{xy}^\infty \right) \right] \\ & + \frac{\kappa - 1}{2\gamma_1} \frac{\sigma_0}{\mu R} \overline{g^2(t)} \quad (26) \end{aligned}$$

where

$$\begin{aligned} \eta &= (2\mu_0 + \lambda_0) / (4R), \\ \eta^{(1)} &= \eta + 0.25\sigma_0/R, \eta^{(2)} = \eta - 0.25\sigma_0/R \\ I_1(s_t, n) &= \int_{-1}^1 \frac{\sqrt{1 - s^2} U_n(s) ds}{(s - s_t)^2} \\ &= \pi (n + 1) \frac{\left(s_t - \sqrt{s_t^2 - 1} \right)^{n+1}}{\sqrt{s_t^2 - 1}} \quad (27) \\ I_2(s_t, n) &= \int_{-1}^1 \frac{\sqrt{1 - s^2} U_n(s) ds}{(s - s_t)^3} \\ &= -\frac{1}{2} I_1(s_t, n) \left[\frac{n + 1}{\sqrt{s_t^2 - 1}} + \frac{s_t}{s_t^2 - 1} \right] \end{aligned}$$

and $s_t = (2t - a - b) / (b - a)$, $\gamma_1 = (b - a) / (\overline{b} - \overline{a})$.

To solve the system (25), (26) and define the unknown coefficients one needs to truncate the series. The displacements and the displacement discontinuities should be truncated as follows:

$$\begin{aligned} \sigma^{\text{inh}}(\tau) &= \sum_{m=2}^{M_h} B_{-m}^{\text{inh}} g^m(\tau) + \sum_{m=0}^{M_h} B_m^{\text{inh}} g^{-m}(\tau) \\ \sigma^{\text{mat}}(\tau) &= \sum_{m=2}^{M_h} B_{-m}^{\text{mat}} g^m(\tau) + \sum_{m=0}^{M_h} B_m^{\text{mat}} g^{-m}(\tau) \\ u(\tau) &= \sum_{m=1}^{M_h-1} A_{-m} g^m(\tau) + \sum_{m=1}^{M_h+1} A_m g^{-m}(\tau) \\ \Delta u^c(s) &= \sqrt{1 - s^2} \sum_{n=0}^{M_c} d_n U_n(s) \quad (28) \end{aligned}$$

Reduction to a linear algebraic system

A system of linear algebraic equations can be obtained by using a Galerkin (weighted residual) method. Multiplying both parts of Eq. (25) by functions $g^p(t)$ ($p = -M_h + 1, \dots, -1, 1, \dots, M_h + 1$) and integrating along the boundary L , one obtains the system of following equations:

$$\begin{aligned}
 & \left[1 + \kappa \left(\frac{\mu_1}{\mu} + p \frac{\eta^{(1)}}{\mu} \right) \right] \frac{A_{-p}}{R} \\
 & - (p + 2) \kappa \frac{\eta^{(2)}}{\mu} \frac{\bar{A}_{(p+2)}}{R} \\
 & + i \gamma_1^p \sum_{n=0}^{M_c} \left\{ -\frac{d_n}{b-a} G_{pn}(\bar{s}_{z_c}) \right. \\
 & - \frac{\bar{d}_n}{\bar{b}-\bar{a}} \left[-\gamma_1 (p+2) G_{(p+2)n}(\bar{s}_{z_c}) \right. \\
 & \left. \left. + p G_{pn}(\bar{s}_{z_c}) + (p+1) \frac{\bar{s}_{z_c} - s_{z_c}}{\gamma_2} G_{(p+1)n}(\bar{s}_{z_c}) \right] \right\} \\
 & = -\frac{\kappa + 1}{4\mu} \left(\sigma_{yy}^\infty - \sigma_{xx}^\infty \right. \\
 & \quad \left. - 2i \sigma_{xy}^\infty \right) \delta_{p1}, \quad p = 1, \dots, M_h - 1 \\
 & \times 4 \left[\frac{\mu_1/\mu}{\kappa_1 - 1} + \frac{\eta}{\mu} + \frac{1}{2} \right] \operatorname{Re} \frac{A_1}{R} \\
 & + i \sum_{n=0}^{M_c} \left[\frac{d_n}{b-a} G_{1n}(s_{z_c}) \right. \\
 & \quad \left. - \frac{\bar{d}_n}{\bar{b}-\bar{a}} G_{1n}(\bar{s}_{z_c}) \right] \\
 & = \frac{\kappa + 1}{4\mu} \left(\sigma_{yy}^\infty + \sigma_{xx}^\infty \right) \\
 & - \frac{\sigma_0}{\mu R} \left[1 + \frac{\mu_1/\mu}{\kappa_1} + p \frac{\eta^{(1)}}{\mu} \right] \frac{A_p}{R} \\
 & - (p - 2) \frac{\eta^{(2)}}{\mu} \frac{\bar{A}_{-(p-2)}}{R} \\
 & + i \sum_{n=0}^{M_c} \frac{d_n}{b-a} G_{pn}(s_{z_c}) \\
 & = 0, \quad p = 2, \dots, M_h + 1 \tag{29}
 \end{aligned}$$

where $\gamma_2 = 2R/(b - a)$, δ_{pq} is the Kronecker delta, and $G_{pn}(z)$ is defined as

$$G_{pn}(z) = \gamma_2^{p-1} \frac{1}{\pi} \int_{-1}^1 \frac{\sqrt{1 - s^2} U_n(s)}{(s - z)^{p+1}} \tag{30}$$

The integral involved in (30) is evaluated analytically using recursive relations, as explained in Wang 2004.

Similarly, multiplying both parts of Eq. (26) by functions $\sqrt{1 - s_i^2} U_q(s_i)$ ($q = 0, \dots, M_c$) and integrating along the boundary L_c , one obtains the following equation ($q = 0, \dots, M_c$):

$$\begin{aligned}
 & 2\operatorname{Re} \frac{A_1}{R} \left[1 - (\kappa - 1) \left(\frac{\mu_1/\mu}{\kappa_1 - 1} + \frac{\eta}{\mu} \right) \right] G_{1q}(\bar{s}_{z_c}) \\
 & - \frac{1}{\gamma_1} \sum_{m=1}^{M_h-1} \frac{A_{-m}}{R} m \left[1 - \frac{\mu_1}{\mu} - m \frac{\eta^{(1)}}{\mu} \right] G_{mq}(s_{z_c}) \\
 & + \sum_{m=1}^{M_h} \gamma_1^m (m + 1) \frac{A_{m+1}}{R} \left\{ \left[1 - \frac{\kappa}{\kappa_1} \frac{\mu_1}{\mu} \right. \right. \\
 & \quad \left. \left. - \kappa (m + 1) \frac{\eta^{(1)}}{\mu} \right. \right. \\
 & \quad \left. \left. - (m - 1)(m + 1) \frac{\eta^{(2)}}{\mu} \right] G_{m+1q}(\bar{s}_{z_c}) \right. \\
 & \quad \left. + (m - 1) \frac{\eta^{(2)}}{\mu} \left[\frac{m - 1}{\gamma_1} G_{m-1q}(s_{z_c}) \right. \right. \\
 & \quad \left. \left. + m \frac{\bar{s}_{z_c} - s_{z_c}}{\bar{\gamma}_2} G_{mq}(\bar{s}_{z_c}) \right] \right\} \\
 & - \sum_{m=1}^{M_h-1} \gamma_1^{m+1} m \frac{\bar{A}_{-m}}{R} \left\{ \left[-\frac{m}{\gamma_1} G_{mq}(\bar{s}_{z_c}) \right. \right. \\
 & \quad \left. \left. - (m + 1) \frac{\bar{s}_{z_c} - s_{z_c}}{\bar{\gamma}_2} G_{m+1q}(\bar{s}_{z_c}) \right. \right. \\
 & \quad \left. \left. + (m + 2) G_{m+2q}(\bar{s}_{z_c}) \right] \left[1 - \frac{\mu_1}{\mu} - m \frac{\eta^{(1)}}{\mu} \right] \right. \\
 & \quad \left. + \kappa (m + 2) \frac{\eta^{(2)}}{\mu} G_{m+2q}(\bar{s}_{z_c}) \right\} \\
 & - \sum_{m=1}^{M_h} \frac{(m - 1)(m + 1) \eta^{(2)}}{\gamma_1} \frac{\bar{A}_{m+1}}{\mu R} G_{m-1q}(s_{z_c}) \\
 & + i(q + 1) \frac{d_q}{b-a} \frac{1}{\bar{\gamma}_2 \gamma_2} \\
 & = \frac{\kappa + 1}{8\mu} \frac{1}{\bar{\gamma}_2 \gamma_2} \left[2\sigma^c(t) - \left(\sigma_{xx}^\infty + \sigma_{yy}^\infty \right) \right. \\
 & \quad \left. - \frac{1}{\gamma_1} \left(\sigma_{yy}^\infty - \sigma_{xx}^\infty - 2i \sigma_{xy}^\infty \right) \right] \delta_{0q} \\
 & + (\kappa - 1) \frac{\sigma_0}{2\mu R} G_{1q}(\bar{s}_{z_c}) \tag{31}
 \end{aligned}$$

Separating real and imaginary parts in Eq. (29) and (31), we get the system of $4M_h + 2M_c + 1$ real linear algebraic equations, where the transposed vector of unknowns is

$$\begin{aligned}
 & \left[\operatorname{Re} A_{-(M_h-1)}, \operatorname{Im} A_{-(M_h-1)}, \dots, \right. \\
 & \operatorname{Re} A_{-1}, \operatorname{Im} A_{-1}, \operatorname{Re} A_1, \operatorname{Re} A_2, \operatorname{Im} A_2, \dots, \\
 & \operatorname{Re} A_{(M_h+1)}, \operatorname{Im} A_{(M_h+1)}, \operatorname{Re} d_0, \operatorname{Im} d_0, \dots, \\
 & \left. \operatorname{Re} d_{M_c}, \operatorname{Im} d_{M_c} \right] \tag{32}
 \end{aligned}$$

Appendix 2

Calculations of the displacements, stresses, strains and stress intensity factors in the system

After substituting expressions (28) into formulae (13), (14) and (15), all integrals can be evaluated analytically. The final expressions for the potentials for the disc (13) and the hole (14) are the same as the corresponding expressions in Mogilevskaya et al. (2008). The final expressions for terms involved in Eq. (15) are as follows

$$\begin{aligned} \varphi_c(z) &= -\frac{i\mu}{\kappa+1} \sum_{n=0}^{M_c} d_n I_0(s_z, n) + f_\varphi(\sigma^c) \\ \psi_c(z) &= \frac{i\mu}{\kappa+1} \sum_{n=0}^{M_c} \left\{ \bar{d}_n I_0(s_z, n) \right. \\ &\quad \left. + \frac{2}{b-a} [\gamma_1(z-a) + \bar{a}] d_n I_1(s_z, n) \right\} \\ &\quad + f_\psi(\sigma^c) \end{aligned} \quad (33)$$

where

$$\begin{aligned} I_0(s_z, n) &= \frac{1}{\pi} \int_{-1}^1 \frac{\sqrt{1-s^2} U_n(s)}{s-z} \\ &= -\left(s_z - \sqrt{s_z^2 - 1} \right)^{n+1} \end{aligned} \quad (34)$$

and the functions $f_\varphi(\sigma^c)$, $f_\psi(\sigma^c)$ are known after one evaluates the integrals from Eq. (15) that contain σ^c .

Resulting potentials define the stresses in the matrix and an inhomogeneity in unique way, as the displacements are defined by the potentials up to some additional terms. These terms correspond to rigid body translations and rotations, and are found the following procedure similar to one described in Mogilevskaya et al. (2008).

The stress intensity factors at the tips of the crack can be calculated from the coefficients of the Chebyshev polynomials by using expressions (17) and (21). The final expressions are the following (Wang et al. 2001):

$$\begin{aligned} (K_1 - iK_2)_a &= -\frac{2\sqrt{2\pi}\mu i \exp(-i\theta_1/2)}{\kappa+1} \sum_{n=0}^{M_c} (-1)^n (n+1) d_n \end{aligned}$$

$$\begin{aligned} (K_1 - iK_2)_b &= -\frac{2\sqrt{2\pi}\mu i \exp(-i\theta_2/2)}{\kappa+1} \sum_{n=0}^{M_c} (n+1) d_n \end{aligned} \quad (35)$$

References

- Chen T, Dvorak GJ, Yu CC (2007) Size-dependent elastic properties of unidirectional nano-composites with interface stresses. *Acta Mech* 188:39–54
- Chuang T-J (1987) Effect of surface tension on the toughness of glass. *J Am Ceram Soc* 70:160–164
- Duan HL, Wang J, Huang ZP, Luo ZY (2005a) Stress concentration tensors of inhomogeneities with interface effects. *Mech Mater* 37:723–736
- Duan HL, Wang J, Huang ZP, Karihaloo BL (2005b) Eshelby formalism for nano-inhomogeneities. *Proc R Soc Lon A461:3335–3353*
- Duan HL, Wang J, Huang ZP, Karihaloo BL (2005c) Size-dependent effective elastic constants of solids containing nano-inhomogeneities with interface stress. *J Mech Phys Solids* 53:1574–1596
- Duan HL, Wang J, Karihaloo BL, Huang ZP (2006) Nanoporous materials can be made stiffer than non-porous counterparts by surface modification. *Acta Mater* 54:2983–2990
- Duan HL, Yi X, Huang ZP, Wang J (2007) A united scheme for prediction of effective moduli of multiphase composites with interface effects. Part I: theoretical framework. *Mech Mater* 39:81–93
- Fang QH, Liu YW (2006) Size-dependent interaction between an edge dislocation and a nanoscale inhomogeneity with interface effects. *Acta Mater* 54:4213–4220
- Fang QH, Li B, Liu YW (2007) Interaction between edge dislocations and a circular hole with surface stress. *Phys Stat Sol B* 244:2576–2588
- Gurtin ME, Murdoch AI (1975) A continuum theory of elastic material surfaces. *Arch Ration Mech Anal* 57:291–323
- Gurtin ME, Murdoch AI (1978) Surface stress in solids. *Int J Solids Struct* 14:431–440
- He LH, Li ZR (2006) Impact of surface stress on stress concentration. *Int J Solids Struct* 43:6208–6219
- Helsing J, Jonsson A (2002) On the accuracy of benchmark tables and graphical results in the applied mechanics literature. *J Appl Mech* 69:80–90
- Huang ZP, Wang J (2006) A theory of hyperelasticity of multiphase media with surface/interface energy effect. *Acta Mech* 182:195–210
- Lim CW, Li ZR, He LH (2006) Size-dependent, non-uniform elastic field inside a nano-scale spherical inclusion due to interface stress. *Int J Solids Struct* 43:5055–5065
- Linkov AM (2002) Boundary integral equations in elasticity theory. Kluwer, Dordrecht
- Linkov AM, Mogilevskaya SG (1998) Complex hypersingular BEM in plane elasticity problems. In: Sladek V, Sladek J (eds) *Singular integrals in boundary element method*. Computational Mechanics Publication, Southampton pp 299–364
- Mi C, Kouris DA (2006) Nanoparticles under the influence of surface/interface elasticity. *Mech Mater Struct* 1:763–791

- Miller RE, Shenoy VB (2000) Size-dependent elastic properties of nanosized structural elements. *Nanotechnology* 11:139–147
- Mogilevskaya SG, Crouch SL (2001) A Galerkin boundary integral method for multiple circular elastic inclusions. *Int J Numer Methods Eng* 52:1069–1106
- Mogilevskaya SG (1996) The universal algorithm based on complex hypersingular integral equation to solve plane elasticity problems. *Comput Mech* 18:127–138
- Mogilevskaya SG, Crouch SL, Stolarski HK (2008) Multiple interacting circular nano-inhomogeneities with surface/interface effects. *J Mech Phys Solids* 56:2327–2928
- Mogilevskaya SG, Linkov AM (1998) Complex fundamental solutions and complex variables boundary element method in elasticity. *Comput Mech* 22:88–92
- Muskhelishvili NI (1959) Some basic problems of the mathematical theory of elasticity. Noordhoff, Groningen
- Oh E-S, Walton JR, Slattery JC (2006) A theory of fracture based upon an extension of continuum mechanics to the nanoscale. *J Appl Mech* 73:792–798
- Phan AV, Gray LJ, Kaplan T (2007) On some benchmark results for the interaction of a crack with a circular inclusion. *J Appl Mech* 74:1282–1284
- Rajapakse YDS (1975) Surface energy and surface tension at holes and cracks. *Int J Fract* 11:57–69
- Sharma P, Ganti S (2002) Interfacial elasticity corrections to size-dependent strain-state of embedded quantum dots. *Phys Stat Sol* 234:R10–R12
- Sharma P, Ganti S (2004) Size-dependent Eshelby's tensor for embedded nano-inclusions incorporating surface/interface energies. *J Appl Mech* 71:663–671
- Sharma P, Ganti S, Bhate N (2003) Effect of surfaces on the size-dependent elastic state of nano-inhomogeneities. *Appl Phys Lett* 82:535–537
- Tian L, Rajapakse RKND (2007a) Analytical solution for size-dependent elastic field of a nanoscale circular inhomogeneity. *J Appl Mech* 74:568–574
- Tian L, Rajapakse RKND (2007b) Elastic field of an isotropic matrix with a nanoscale elliptical inhomogeneity. *Int J Solids Struct* 44:7988–8005
- Tian L, Rajapakse RKND (2007c) Finite element modelling of nanoscale inhomogeneities in an elastic matrix. *Comp Mater Sci* 41:44–53
- Thomson R, Chuang T-J, Lin I-H (1986) The role of surface stress in fracture. *Acta Metall* 34:1133–1143
- Wang J (2004) Numerical modeling of elastic materials with inclusions, holes, and cracks. Ph.D. Thesis. University of Minnesota, Minneapolis
- Wang J, Mogilevskaya SG, Crouch SL (2001) A Galerkin boundary integral method for nonhomogeneous materials with cracks. In: Elsworth D, Tinucci JP, Heasley KA (eds) *Rock mechanics in the national interest*. Balkema, Rotterdam pp 1453–1460
- Wang J, Mogilevskaya SG, Crouch SL (2003) Benchmark results for the problem of interaction between a crack and a circular inclusion. *J Appl Mech* 70:619–621
- Wu CH (1999) The effect of surface stress on the configurational equilibrium of voids and cracks. *J Mech Phys Solids* 47:2469–2492
- Wu CH, Wang ML (2001) Configurational equilibrium of circular-arc cracks with surface stress. *Int J Solids Struct* 38:4279–4292
- Yang FQ (2004) Size-dependent effective modulus of elastic composite materials: spherical nanocavities at dilute concentrations. *J Appl Phys* 95:3516–3520
- Zhang WX, Wang TJ (2007) Effect of surface energy on the yield strength of nanoporous materials. *Appl Phys Lett* 90, Art. No. 063104